Supplementary Materials

Feasibility Study of Magnetic Sensing for Detecting Single-Neuron Action Potentials

Denis Tonini, Kai Wu, Renata Saha, Jian-Ping Wang*

Department of Electrical and Computer Engineering, University of Minnesota, Minneapolis, MN 55455, United States

*Corresponding author Email: jpwang@umn.edu (J.-P. W)

S1. Magnetic Fields Generated by Worm Axon

A simplified geometry of a giant squid axon is simulated using the LFPy software derived from the NEURON software (1–5), validating the experimental magnitude of the magnetic field generated in the vicinity of a neural axon (6), where the diameter and synaptic weight reproduce a current intensity in the order of ~100-500 nA similar to the results published in the literature by Suszkiw et al. and Holz et al. (7,8). By comparing the *in-vivo* experimental results obtained by Barry et al. for *M. Infundibulum* with the theoretical simulation illustrated in Fig. S1, it is possible to correlate a similar magnitude of the magnetic field, considering an increase of the synaptic strength in accordance with experimental expectations (1,2). Therefore, it is possible to validate the efficacy of the theoretical simulation concerning the estimation of the magnetic field generated by neural activities, as well as single-neuron action potentials. Fig. S1(a) represents the location of the synapse with respect to the position of the sensor, whereas Fig. S1(b) illustrates the maximum magnitude of the magnetic field in the order of ~500 pT, and Fig. S1(c) shows a synaptic potential ΔV_{soma} of around 30 mV equivalent to experimental measurements. Furthermore, Fig. S1(d) depicts the maximum synaptic current in the order of 150 nA in accordance with experimental results available in the literature (7,8).

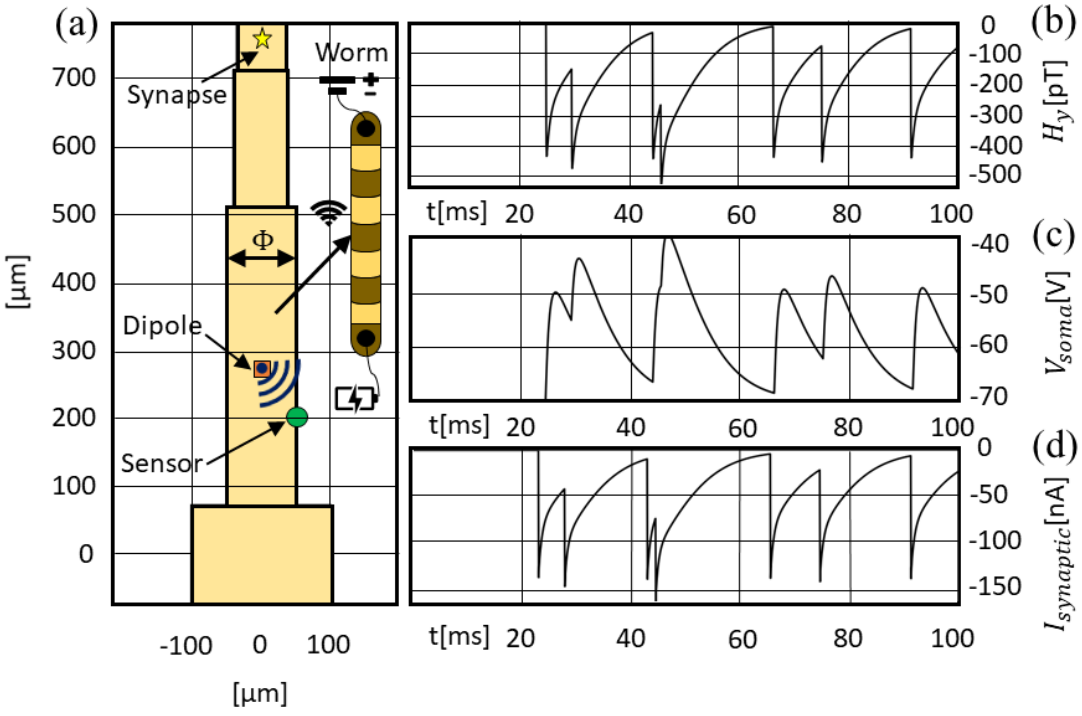

Figure S1. Giant squid axon simulated in LFPy. (a) Simplified geometry of an axon during stimulation through microelectrodes. The sensor, the dipole, and the synapse location are represented by the green, orange, and yellow shapes (6). (b) Magnetic field measured along the y-direction of the axon (Hy) in pT. (c) Soma potential at the sensor location. (d) Synaptic current at the sensor location.

S2. Electrochemical Analysis of Neuronal Activities

During an evoked action potential in neuronal regions, diffusion phenomena are limited by the ionic transport taking place within the membrane. In addition, in the case of electrode-based neurostimulation and sensing, the physiological properties of the neuronal tissue are affected by local nonequilibrium perturbations attributed to the direct contact with the metallic plates of the electrode, according to the physics described by the Marcus theory for electron transfer (9,10). Furthermore, the heat transfer arising from the circulatory system is also responsible for temperature gradients provoking microfluidic effects, such as convection and cavitation around the microelectrodes, which causes hydrodynamic perturbations in the chemical potential at a distance from the electrode beyond ~10 μm (11–17). Therefore, electrode-based neurostimulation perturbs the equilibrium of neuronal tissue abating the high-frequency response because of impedance effects caused by the direct contact of the neuronal tissue and the cerebrospinal fluid with the conductive metallic plate of the implanted microelectrodes. At the surface of the electrode, diffusion phenomena limit the ability to sense and stimulate action potentials through implanted non-contactless microelectrodes in agreement with the Cottrell equation and Fick's laws of diffusion. The derivation of the second Fick's law of diffusion in terms of concentration is stated as:

$$C_{OX}(x,t) = C_{OX}^{*}\left\{erf\left[\frac{x}{2\sqrt{D_{OX}t}}\right]\right\} \quad (1),$$

For the following boundary conditions:

$$\begin{cases} C_{OX}(\infty,t) = C_{OX}^{*} = C_{Bulk} \\ C_{OX}(x,t=0) = C_{OX}^{*} \\ C_{OX}(x_0,t>0) = 0 \end{cases} \quad (2),$$

Where: t is the time, x the distance from the electrode; C_{OX}^{*} is the initial concentration of the oxide species derived from the Butler-Volmer equation assumed equal to C_{Bulk} in case of an ideally infinite continuous system without depletion; D_{OX} the diffusivity constant for oxidation reactions in cm^2/s; x_0 the initial distance from the electrode; x the distance from the electrode, and $erf\{*\}$ represents the error function. The same approach is valid for reduction reactions. Setting the distance equal to $x = \sqrt{D_{ox}t}$ and assuming a diffusivity constant in the order of $D_{ox} = 10^{-5}$ [cm^2/s], it is possible to approximate the concentration as:

$$C_{OX}(x,t) = C_{OX}^{*}\{erf[0.5]\} \approx 0.525\, C_{OX}^{*}$$

Therefore, considering $x = \sqrt{D_{ox}t}$, it is possible to estimate the concentration profile as a time-domain function for different distances to highlight the temporal and spatial limitations of electrode-based stimulation and sensing, as shown in Table S1. The diffusion occurring around the neuronal tissue is dependent on the physical properties of the system and the time delay arising from the electronic instrumentation. If the sampling period is in the order of ~1μs, it is necessary to sense at a maximum

distance of 30 nm to avoid diffusion limitations. Therefore, electrode-based stimulation has a limited temporal resolution. The convection phenomena occurring nearby the electrode are provoked by the heat transfer arising from the circulatory system and the electrolyte solution, where the neurons are submerged. Considering a time resolution of 1 ms, the diffusivity is dominant up to 1 µm, far below the distance to the electrode (18).

Table S1. Temporal limitations of electrical-based stimulation

Time	1s	1ms	1µs
Space	30µm	1µm	30nm

Non-contactless electrode-based sensing and stimulation techniques are temporally limited by the ionic transport and diffusion phenomena, whereas contactless magnetic stimulation is limited by the permeability and permittivity of the system for non-relativistic electromagnetic models according to the Maxwell equations. The result is valid for short distances both in planar and spherical electrodes.

S3. Graphical Interface.

The interface in Fig. S2 integrates MATLAB and the NEURON compiler by automatically setting the parameters in the file and running the compiler. The current in Fig. S2 counts only the capacitive term and does not include further contributions. By changing the membrane capacitance and resistance, it is possible to measure the charge response to an action potential, as well as the magnetic field generated by the capacitive term according to the Biot-Savart law. The refractory period is estimated when the stimulus occurs. The same approach can also be applied for brain sensing. The main advantage of this interface is the adaptability for controlling the system through machine-learning techniques to distinguish positive and negative action potentials, image processing techniques to map the neuronal geometry, and parallelized computing to increase the performance for a network of neuronal cells. In this simulation, the cell capacitance is supposed to be 147.11 ± 13.29 pF (19). The radius of the axon is in accordance with the results published in the literature (20–22). It is possible to change the main parameters such as the capacitance, the resistance, the inductance of the micro-coil, and the current pulse specifics, as well as the time duration, the membrane characteristics, and the resting potential. The radius of the axon is considered in the order of ~100 µm. For standard hippocampal axons (0.1 µm), it translates to a maximum magnetic field in the order of 2–3 nT for a bundle of neuronal cells. The map of the electric field is derived from Saha et al. (23).

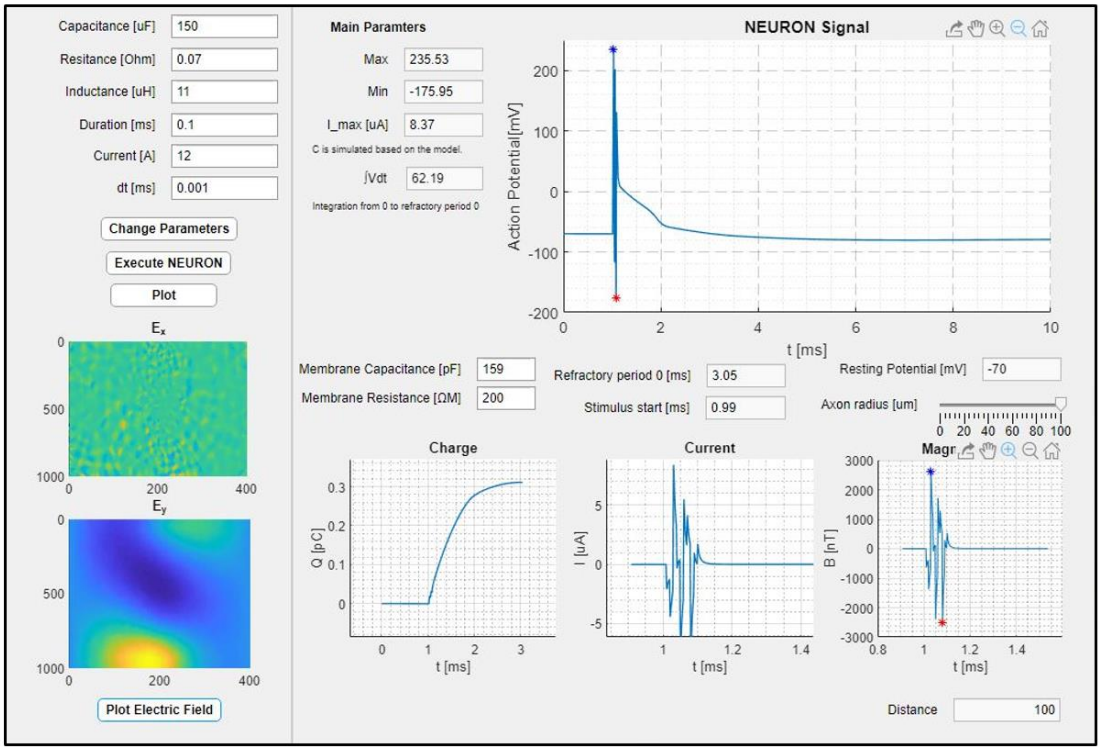

Figure S2. MATLAB graphical interface to simulate the parameters deriving from NEURON (23,24).

S4. Source Code LFPy simulation available on the GitHub LFPy page under GNU license.

The following modifications are implemented to store the simulation data:

```
#for i in range(-500, 500, 100):
for j in range(-500, 500, 50):
  for n in range(-1200,400, 50):
    # Define sensor site, instantiate MEG object, get transformation matrix
    sensor_locations = np.array([[n, 0, j]])
    meg = MEG(sensor_locations)
    M = meg.get_transformation_matrix(dipole_location)
    # compute the magnetic signal in a single sensor location:
    H = M @ current_dipole_moment.data
 #   # Open the file in append & read mode ('a+')
 #   with open("t.csv", "ab") as myfile:
 #     np.savetxt(myfile, cell.tvec, delimiter=',')
 #   with open("V.csv", "ab") as myfile:
 #     np.savetxt(myfile, cell.somav, delimiter=',')
 #   with open("I_syn.csv", "ab") as myfile:
 #     np.savetxt(myfile, syn.i, delimiter=',')
 #   with open("H.csv", "ab") as myfile:
 #     np.savetxt(myfile, H[0].T, delimiter=',')

#np.savetxt('V.csv', cell.somav, delimiter=',')
#np.savetxt('I_syn.csv', syn.i , delimiter=',')
#np.savetxt('myfile.csv', H[0].T, delimiter=',')
```

The following code, excluding the part to extract the data, is publicly available under the GNU General Public License v3 at https://github.com/LFPy/LFPy/blob/master/LFPy/eegmegcalc.py, Copyright 2020 Computational Neuroscience Group NMBU (1,2). The network of neuronal cells is based on the file example_network.py in LFPy, copyright 2017 Computational Neuroscience Group NMBU under the GNU General Public License. The following code is publicly available under the GNU General Public License v3 at: https://github.com/LFPy/LFPy/blob/master/examples/ example_network/example_network.py (1,2).

Source Code LFPy simulation available on the GitHub LFPy page under GNU license.

The following modification are implemented to store the simulation data:

```
if i == 2 & j==2:
    np.savetxt('tz.csv', t[inds], delimiter=',')
    np.savetxt('pz.csv', current_dipole_moment.data[name][i, inds], delimiter=',')
with open("x.csv", "ab") as myfile:
  np.savetxt(myfile, [cell.x[1, 0], cell.x[-1, -1]], delimiter=',')
with open("y.csv", "ab") as myfile:
  np.savetxt(myfile, [cell.y[1, 0], cell.y[-1, -1]], delimiter=',')
with open("z.csv", "ab") as myfile:
  np.savetxt(myfile, [cell.z[1, 0], cell.z[-1, -1]], delimiter=',')
```

The following code, excluding the part to extract the data, is publicly available under the GNU General Public License at: https://github.com/LFPy/LFPy/blob/master/examples/example_network/example_network.py, Copyright 2017 Computational Neuroscience Group, NMBU. LFPy is used to run the code (1,2). Once the vectors are extracted, MATLAB is used to plot the data.

References

1. Hagen E, Næss S, Ness TV, Einevoll GT. Multimodal Modeling of Neural Network Activity: Computing LFP, ECoG, EEG, and MEG Signals With LFPy 2.0. Front Neuroinformatics. 2018;12:92.

2. Lindén H, Hagen E, Leski S, Norheim E, Pettersen K, Einevoll G. LFPy: a tool for biophysical simulation of extracellular potentials generated by detailed model neurons. Front Neuroinformatics. 2014;7:41.

3. Carnevale NT, Hines ML. The NEURON Book [Internet]. Cambridge: Cambridge University Press; 2006 [cited 2023 Jan 11]. Available from: https://www.cambridge.org/core/books/neuron-book/7C8D9BD861D288E658BEB652F593F273

4. Hines M. The neurosimulator NEURON. Methods Neuronal Model Ed C Koch Segev Camb MA MIT Press. 1998;129–36.

5. Hines M, Carnevale N, Carnevale N, Carnevale N. NEURON: a tool for neuroscientists. The Neuroscientist. 2001;7:123–35.

6. Barry JF, Turner MJ, Schloss JM, Glenn DR, Song Y, Lukin MD, et al. Optical magnetic detection of single-neuron action potentials using quantum defects in diamond. Proc Natl Acad Sci. 2016 Dec 6;113(49):14133–8.

7. Holz RW, Fisher SK. Chapter 12 - Synaptic Transmission and Cellular Signaling: An Overview. In: Brady ST, Siegel GJ, Albers RW, Price DL, editors. Basic Neurochemistry (Eighth Edition) [Internet]. New York: Academic Press; 2012 [cited 2022 Feb 5]. p. 235–57. Available from: https://www.sciencedirect.com/science/article/pii/B9780123749475000122

8. Suszkiw JB. Chapter 32 - Synaptic Transmission. In: Sperelakis N, editor. Cell Physiology Source Book (Fourth Edition) [Internet]. San Diego: Academic Press; 2012 [cited 2022 Feb 5]. p. 563–78. Available from: https://www.sciencedirect.com/science/article/pii/B9780123877383000329

9. Roy S, Baer MD, Mundy CJ, Schenter GK. Marcus Theory of Ion-Pairing. J Chem Theory Comput. 2017 Aug 8;13(8):3470–7.

10. Mayer JM. Understanding Hydrogen Atom Transfer: From Bond Strengths to Marcus Theory. Acc Chem Res. 2011 Jan 18;44(1):36–46.

11. Baltes N, Thouin L, Amatore C, Heinze J. Imaging Concentration Profiles of Redox-Active Species with Nanometric Amperometric Probes: Effect of Natural Convection on Transport at Microdisk Electrodes. Angew Chem Int Ed. 2004;43(11):1431–5.

12. Amatore C, Szunerits S, Thouin L, Warkocz JS. The real meaning of Nernst's steady diffusion layer concept under non-forced hydrodynamic conditions. A simple model based on Levich's seminal view of convection. J Electroanal Chem. 2001 Mar 16;500(1):62–70.

13. Kim S, Normann RA, Harrison R, Solzbacher F. Preliminary Study of the Thermal Impact of a Microelectrode Array Implanted in the Brain. In: 2006 International Conference of the IEEE Engineering in Medicine and Biology Society. 2006. p. 2986–9.

14. Rohatgi P, Langhals NB, Kipke DR, Patil PG. In vivo performance of a microelectrode neural probe with integrated drug delivery. Neurosurg Focus. 2009 Jul;27(1):E8.

15. Takmakov P, Zachek MK, Keithley RB, Bucher ES, McCarty GS, Wightman RM. Characterization of Local pH Changes in Brain Using Fast-Scan Cyclic Voltammetry with Carbon Microelectrodes. Anal Chem. 2010 Dec 1;82(23):9892–900.

16. Jaquins-Gerstl A, Michael AC. Comparison of the brain penetration injury associated with microdialysis and voltammetry. J Neurosci Methods. 2009 Oct 15;183(2):127–35.

17. Han M, McCreery DB. A new chronic neural probe with electroplated iridium oxide microelectrodes. In: 2008 30th Annual International Conference of the IEEE Engineering in Medicine and Biology Society. 2008. p. 4220–1.

18. Electrochemical Methods: Fundamentals and Applications, 2nd Edition | Wiley [Internet]. Wiley.com. [cited 2022 Mar 25]. Available from: https://www.wiley.com/en-us/Electrochemical+Methods%3A+Fundamentals+and+Applications%2C+2nd+Edition-p-9780471043720

19. Milior G, Di Castro MA, Sciarria LP, Garofalo S, Branchi I, Ragozzino D, et al. Electrophysiological Properties of CA1 Pyramidal Neurons along the Longitudinal Axis of the Mouse Hippocampus. Sci Rep. 2016 Dec 6;6(1):38242.

20. Veraart J, Nunes D, Rudrapatna U, Fieremans E, Jones DK, Novikov DS, et al. Noninvasive quantification of axon radii using diffusion MRI. de Lange FP, Forstmann B, Forstmann B, Jbabdi S, Mulkern R, editors. eLife. 2020 Feb 12;9:e49855.

21. Innocenti GM, Caminiti R, Aboitiz F. Comments on the paper by Horowitz et al. (2014). Brain Struct Funct. 2015 May 1;220(3):1789–90.

22. Liewald D, Miller R, Logothetis N, Wagner HJ, Schüz A. Distribution of axon diameters in cortical white matter: an electron-microscopic study on three human brains and a macaque. Biol Cybern. 2014 Oct 1;108(5):541–57.

23. Saha R, Faramarzi S, Bloom RP, Benally OJ, Wu K, Girolamo A di, et al. Strength-frequency curve for micromagnetic neurostimulation through EPSPs on rat hippocampal neurons and numerical modeling of magnetic microcoil (μcoil) [Internet]. 2021 Dec [cited 2022 Jan 7] p. 2021.11.30.470598. Available from: https://www.biorxiv.org/content/10.1101/2021.11.30.470598v1

24. Pashut T, Wolfus S, Friedman A, Lavidor M, Bar-Gad I, Yeshurun Y, et al. Mechanisms of Magnetic Stimulation of Central Nervous System Neurons. PLOS Comput Biol. 2011 Mar 24;7(3):e1002022.